Nanoscale

Single Molecule Analysis of Structural Fluctuations in DNA Nanostructures

Journal:	*Nanoscale*
Manuscript ID	NR-ART-05-2019-003826.R1
Article Type:	Paper
Date Submitted by the Author:	30-Aug-2019
Complete List of Authors:	Jepsen, Mette; Aarhus University, Interdisciplinary nanoscience center (iNANO) ; Aarhus University, Department of Molecular Biology and Genetics Sørensen, Rasmus; Aarhus University, Interdisciplinary nanoscience center (iNANO); Aarhus University, Department of Molecular Biology and Genetics Maffeo, Christopher; University of Illinois at Urbana-Champaign, Department of physics Aksimentiev, Aleksei; University of Illinois at Urbana-Champaign, Department of Physics Kjems, Jørgen; Aarhus University, Interdisciplinary nanoscience center (iNANO) ; Aarhus University, Departement of Molecular Biology and Genetics Birkedal, Victoria; Aarhus University, Interdisciplinary nanoscience center (iNANO) ; Aarhus University, Department of Chemistry

ARTICLE

Single Molecule Analysis of Structural Fluctuations in DNA Nanostructures

Received 00th January 20xx,
Accepted 00th January 20xx

DOI: 10.1039/x0xx00000x

Mette D. E. Jepsen[a,b], Rasmus Schøler Sørensen[a,b], Christopher Maffeo[c], Aleksei Aksimentiev[c], Jørgen Kjems[a,b], Victoria Birkedal[a,d]*

DNA origami is an excellent tool for building complex artificial nanostructures. Functionalization of these structures provides the possibility of precise organization of matter at the nanoscale. In practice, efforts in this endeavour can be impeded by electrostatic repulsion or other dynamics at the molecular scale, resulting in uncompliant local structures. Using single molecule FRET microscopy combined with coarse-grained Brownian dynamics simulations, we investigated here the local structure around the lid of a DNA origami box, which can be opened by specific DNA keys. We found that FRET signals for the closed box depend on buffer ion concentrations and small changes to the DNA structure design. Simulations provided a view of the global and local structure and showed that the distance between the box wall and lid undergoes fluctuations. These results provide methods to vizualise and improve the local structure of three-dimensional DNA origami assemblies and offer guidance for exercising control over placement of chemical groups and ligands.

Introduction

Due to the unique predictability of Watson–Crick base pairing, DNA can be used to construct pre-defined artificial structures ranging from nanometers to micrometers in size with a large variety of shapes.[1] The dynamics of these structures are programmable through DNA hybridization and thereby these structures can serve as functional molecular devices.[2] Examples of applications include nanorobotics arms based on a DNA actuator with 11 states,[3] DNA origami nano-containers as programmable delivery devices with the potential to respond to cellular signals,[4, 5] and DNA devices for molecular computing applications.[6, 7] Many applications have very stringent structural requirements, not just for the overall structure (size and shape), but also for the local substructure given by the distance between neighboring DNA helices, which can play an essential role for the precise positioning of ligands. A fundamental feature of DNA nanotechnology is the promise of accurate, predictable spatial positioning of DNA and other components. Yet, unexpected flexing and dynamics of the DNA double-helices may produce structures that deviate significantly from the expected design. Uncontrolled distortion of local substructures can have a detrimental effect for many applications, resulting in suboptimal outputs due to leakiness of DNA based containers or biased signals based on nanoscale distances used to monitor conformational changes and molecular processes in DNA nanotechnology. Nanoscale organization of fluorescent matter on static DNA origami structures has been reported with distance accuracy as little as 1.5 nm,[8] demonstrating the general feasibility of having large DNA devices with precise control of the local structure. However, many reconfigurable DNA devices have a more flexible structure than predicted in their design.

Hollow, three-dimensional DNA structures have been reported in different sizes and shapes,[4, 9-12] and proposed as DNA containers and platforms for DNA computation, sensing, control of enzymatic reactions and drug delivery.[4, 7, 13, 14] A foundational example is a DNA box with a lid that can open in response to specific oligonucleotide keys, where lid opening was measured by Förster resonance energy transfer (FRET) spectroscopy.[4] The FRET process allows measuring distance changes with high sensitivity and is used to monitor conformational changes of reconfigurable DNA origami structures.[15-17] As predicted, higher FRET efficiencies were reported for DNA boxes in the closed state compared to the open states. However, the FRET efficiency only changed from ~0.2 in the closed state to ~0.0 in the open state. The closed state FRET efficiency was thus much smaller than expected according to the DNA origami design,[4] indicating that the local structure of the closed DNA box did not conform to the expected structure. The same phenomenon has been observed in other box-like DNA structures.[7, 10]

Here, we investigate the local structure near the lid and opening mechanism of the original DNA box[4] by using fluorescence spectroscopy, single molecule FRET microscopy (smFRET), and Brownian dynamics (BD) simulations. Our FRET experiments probe the local structure around the lid of the closed box, which is sensitive to magnesium concentration and to subtle changes in the DNA origami design. Increasing magnesium concentration decreases electrostatic repulsion and leads to a

[a] Interdisciplinary Nanoscience Center (iNANO), Aarhus University, Aarhus, Denmark. E-mail: vicb@inano.au.dk
[b] Department of Molecular Biology and Genetics, Aarhus University, Aarhus, Denmark.
[c] Center for the Physics of Living Cells, Department of Physics, University of Illinois at Urbana Champaign, 1110 West Green Street, Urbana, Illinois 61801.
[d] Department of Chemistry, Aarhus University, Aarhus, Denmark.
†Electronic Supplementary Information (ESI) available: See DOI: 10.1039/x0xx00000x

tighter closure of the lid of the DNA box structure. Box opening was functional in the full range of magnesium concentrations investigated in this study (0.0125–1.0 M Mg^{2+}). Experimental measurements are complemented by coarse-grained BD simulations that show the box structure in the original design deviates from its idealized orthonormal design and undergoes ~5 nm fluctuations at the interface between the box wall and lid. Small changes in the DNA origami box design allowed significantly decreasing these fluctuations in a more rigid structure. Our work provides methods to determine and control the local structure of large flexible DNA origami structures.

Experimental

DNA assembly and purification:

DNA origami boxes were prepared following original procedures.[4] Briefly, M13 with a concentration of 16 nM and 5 times excess of staple strands in TAE-Mg2+ buffer (40 mM Tris-acetate with 1 mM EDTA, pH 8.3 (Invitrogen) containing 12.5 mM $MgCl_2$ (Sigma-Aldrich)) were assembled by heating to 95 °C and slowly cooling to room temperature in an 8 h process. Similar procedures were used for the modified boxes (see ESI). Four staple strands on the bottom of the box were biotin-labelled on the 3'-end using Terminal Deoxynucleotidyl Transferase (TdT, Roche), as previously described.[18] The annealed samples were purified using S-400 spin columns (GE Healthcare Life Sciences).

Labelled DNA double stranded controls (see ESI for sequences) were annealed in TAE-Mg^{2+} buffer at 90°C for 5 minutes and left to cool slowly over several hours.

Fluorescence spectroscopy:

Fluorescence spectra were recorded on a Fluoromax 3 fluorimeter (Horiba Jobin-Yvon) using 65 µL quartz cuvettes at 25°C. Cy3 and Cy5 fluorescence were excited at 530 nm and 600 nm, respectively. DNA box concentration was ~20 nM. The entrance and exit slits were 5 nm, and the integration time was 0.5 s. Relative FRET efficiencies were determined using the (ratio)A method.[19]

smFRET

smFRET experiments were performed on surface immobilized DNA box structures with prism based total internal reflection fluorescence microscopy. DNA boxes with four biotins on the opposite surface of the box lid were surface immobilized onto the quartz coverslide chamber via BSA-biotin streptavidin linkage at ~20 pM concentration. Excess sample was washed out with buffer after 5 min incubation. The buffer was thereafter exchanged with imaging buffer (20 mM Tris-HCl pH 7.5 (Sigma Aldrich), 100 mM KCl (Sigma Aldrich)) with appropriate $MgCl_2$ concentration and an oxygen scavenging system (1mM Trolox (Sigma Aldrich), 16.67 u/ml glucose oxidase (Sigma Aldrich), 260 u/ml catalase (Sigma Aldrich), and 4.5 mg/ml β-D-(+)glucose (Sigma Aldrich)), and measurements were performed. DNA box opening was imaged following the addition of 5 nM DNA keys to the coverslide chamber.

The samples were illuminated using alternating laser excitation (ALEX) of the donor and acceptor fluorophores at 514 and 630 nm, and fluorescence was detected using an inverted wide-field microscope (Zeiss) coupled to an EMCCD camera (Andor, iXon3 897). The integration time was 200 ms per image, and the EM gain used was 100.

Data analysis was carried out in iSMS (version 1.03) using MATLAB (MathWorks).[20] Co-localized donor/acceptor spots were identified and the corresponding fluorescence time traces analyzed. Data not corresponding to single molecules, that either showed multistep bleaching or high fluorescence intensities, were removed from the analysis. FRET efficiencies were ratiometrically determined after background and filter corrections using Equation 1:

$$E = \frac{F_{A|D}}{F_{A|D} + \gamma I_{D|D}} \qquad (1)$$

where $F_{A|D}$ is the acceptor signal after donor excitation arising from FRET, $I_{D|D}$ is the donor fluorescence intensity and γ is a correction factor that accounts for the different quantum yields and detection efficiencies of the donor and acceptor fluorophores. γ was determined directly from the measurements from traces where the acceptor bleached first.[21] We obtained average γ-values of 2.5 ± 0.4 for the original box, of 1.7 ± 0.1 for the original box with both fluorophores situated on the same face of the box and 1.9 ± 0.2 for the linked box: γ-values did not depend on magnesium concentration. smFRET histograms were built based on the data arising from molecules containing both active donor and acceptor fluorophores with each frame yielding a count. Histograms contained ~100 or more molecules, unless otherwise specified, and were fitted by Gaussian distributions to determine FRET efficiencies of the peak values. Uncertainties for determined FRET efficiencies are mainly due to uncertainties from γ-value determination.

BD simulations:

The coarse-grained BD simulations were performed using an in-house-developed and GPU-accelerated simulation package, ARBD,[22] and a recently developed workflow for modeling DNA origami systems as previously described.[23] Briefly, the model was constructed by importing Cadnano 2.5[24] as a Python module to read and convert the origami box design to low- (~5 base pairs per bead) and high-resolution (2 beads per base pair) polymer models, which were respectively used for initial structural relaxation and for monitoring the distance between FRET labeling sites. Harmonic bonded potentials were derived from the experimentally determined bending and torsional persistence lengths (50 and 90 nm, respectively).[25, 26] Solvent was represented implicitly by non-bonded interactions between beads that were tuned against a potential of mean force for the interaction between a pair of isolated dsDNA fragments in 100 mM $MgCl_2$.[27] Crossover bonds between adjacent helices were modeled using a harmonic potential designed to reproduce a bond–length distribution previously extracted from all-atom simulations of a DNA origami object (Gaussian with ~1.8 nm center and ~0.3 nm width).[28]

The simulations of the box began with brief structural relaxation using the low-resolution model, starting from an idealized geometry. The high-resolution model was mapped into the configuration of the low-resolution model after a 100 ns

simulation where bonds longer than 10 nm (*i.e.* between the box faces) were ignored. Subsequent simulation of the low-resolution model lasted five microseconds, requiring approximately two days of continuous simulation on a workstation equipped with a GTX 1080Ti GPU. We note that the effective timescale of the simulation is expected to be significantly longer than five microseconds because the free energy landscape of the coarse-grained model is much smoother than an equivalent atomistic system.[29] The precise speed-up has not been determined.

Results and Discussion

The design of the DNA origami box enables the lid to be opened in response to specific oligonucleotide inputs.[4] In its closed position, the lid is held closed by two DNA locks. For each lock, one strand of the double helix is attached to the front face of the box, and the other strand to the lid. The two DNA strands are not of equal length, which allows opening of the lid through DNA strand displacement by adding external oligonucleotide keys (Figure 1). Fluorophores are placed close to the front edge in the middle of the lid and on the corresponding opposing box face on attachment points separated by 3.2 nm in the closed box design. As the fluorophores at these positions are expected to point towards each other, they should be very close to each other (Figure S1, ESI). This fluorophore configuration enables FRET between the fluorophores to be used to sense changes in box structure in response to lid opening. The FRET efficiency of the closed state was previously determined to be only 0.27.[4] This value naively corresponds to an average distance between the two fluorophores of more than 6 nm, far greater than expected from the design of the structure. The discrepancy could be due to the lid not being as tightly closed as expected or to a structurally heterogeneous sample containing both closed and open structures.

smFRET microscopy allows monitoring conformational changes in real time while obtaining a view of conformational distributions and sample heterogeneity. smFRET histograms of DNA boxes before DNA key addition showed a relatively narrow FRET efficiency distribution centered at ~0.15 and no higher FRET peaks (Figure 1b). We did not observe two distinct subpopulations of opened and closed boxes, indicating that the detected FRET efficiency arises primarily from a homogeneous closed box population. After addition of DNA keys, only one distribution, centered around zero, is observed in the smFRET histogram. This change reflects a general increase in the distance between donor and acceptor due to box lid opening, which is also observed in single molecule time-traces (Figure S2, ESI). The photophysics of the fluorophores and their interaction with each other and with the DNA scaffold can also influence the FRET efficiency.[30-34] In about 70% of time traces, we observed an increase in Cy5 fluorescence quantum yield following box opening (Figure S2, ESI). DNA in the vicinity of the Cy5 fluorophore or the presence of a close-by Cy3 fluorophore are likely candidates to quench Cy5 fluorescence, which was observed to be quenched by about 30%. Both effects were previously reported to affect Cy5 quantum yield.[30, 35] Heavy fluorescence quenching can lead to signal disappearance when donor and acceptor fluorophores are very close to each other.[36] However, since the quenching was relatively small, it is unlikely that it could mask stable high FRET states. Thus, the FRET efficiency of ~0.2 found by both ensemble and single molecule fluorescence studies arises from closed boxes, and this low value suggests that the lid is not as tightly closed as expected (Figure 1a, 2a and Figure S1, ESI).

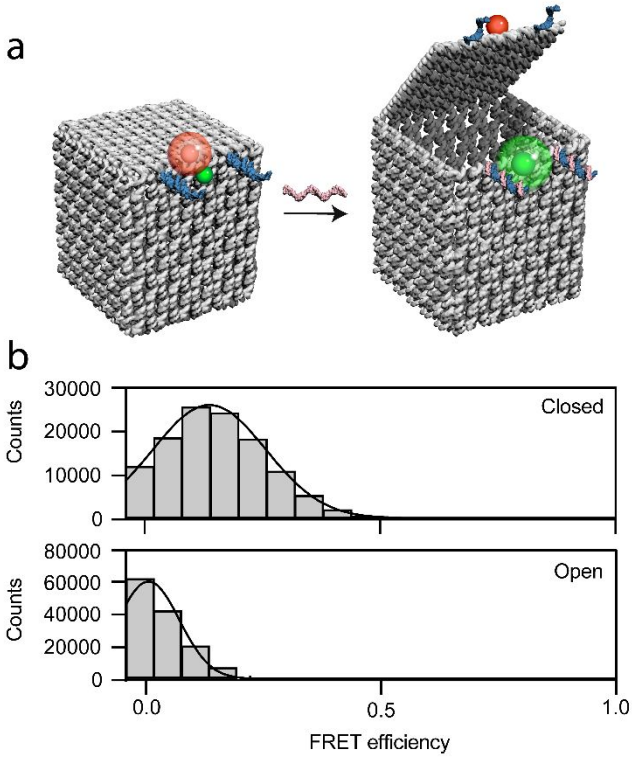

Figure 1: (a) 3D representation of the closed and open DNA box.[4] Fluorophores, Cy5 and Cy3, are marked in red and green, respectively, DNA locks are marked in blue and DNA keys in red. (b) Single molecule smFRET histograms of the original DNA box before and after addition of DNA keys.

To obtain a detailed view of the structure we employed a BD model recently developed for DNA origami nanostructures using a combination of known DNA polymer properties and results from all-atom molecular dynamics simulations (see Experimental for details of the model).[25-27] Starting from an idealized geometry realized by placing all helices parallel to one another (Figure 2a), the simulation quickly (within 100 ns) produced a model of a closed DNA box at ~5 base pair per bead resolution. The model was converted into a higher, 2 beads per base pair resolution for a subsequent 5-µs long simulation. During the simulation, the box lid developed a convex curvature (Figure 2b) while the helices at the sides of the box continually explored different local configurations. Supplementary Information Movie 1 illustrates this simulation trajectory. Despite the strong curvature of the lid, the simulated DNA density (Figure 2c) is found to be consistent with the 3D reconstruction of the electron density from transmission electron microscopy (Figure 2d).[4] The simulations revealed that the distance between fluorophore attachment sites fluctuated

between 6 and 12 nm (Figure 2e), in qualitative agreement with the relatively low FRET efficiency observed experimentally. These fluctuations could be influenced by electrostatic repulsions of the negative charges in the DNA backbone. To test this hypothesis experimentally, we used a gradual increase in cationic strength to influence electrostatic repulsions within the box.

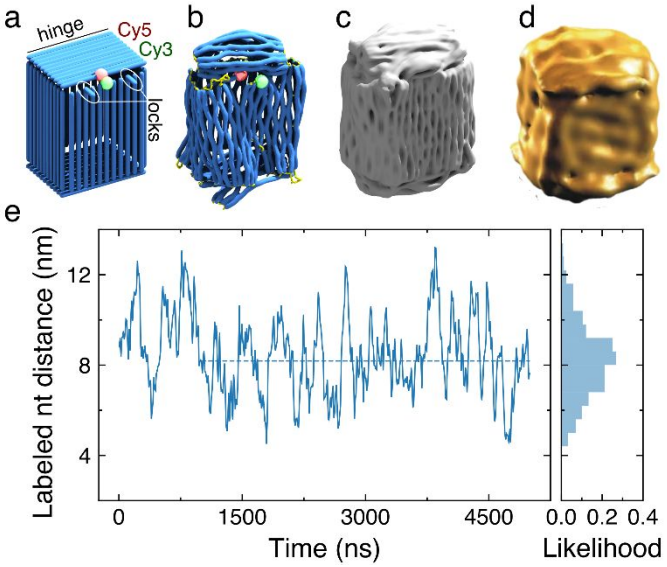

Figure 2: (a) Idealized three-dimensional configuration of the DNA box. (b) Configuration of the DNA box after ~5 µs of BD simulation. Double- and single-stranded DNA are depicted as blue tubes and yellow lines, respectively. (c) Simulated DNA density after averaging over D_2 symmetry and the simulation trajectory. (d) Three dimensional reconstruction of the electron density of a DNA box derived from transmission electron microscopy and reproduced with permission,[4] from MacMillan Publishers Ltd: Nature (Andersen et al.,2009) © (2009). (e) Time series of the distance between nucleotides labeled with fluorescent dyes. The dashed line shows the average value of the distance from the last 4 µs of the simulation trajectory. The histogram on the right depicts the distribution of the distance during the same time window.

The effect of Magnesium on the DNA Origami Box

Mg^{2+} has been shown to effectively shield the negative charges in the backbone of DNA,[37] and since it is already present at 12.5 mM in the assembly buffer (TAE Mg^{2+}), it was chosen as cation. The effect of magnesium on the DNA origami box was studied using ensemble FRET measurements, where a box sample was exposed to variable Mg^{2+} concentrations. The FRET efficiency is observed to increase with increasing Mg^{2+} concentration (Figure S3, ESI). This could be due to the lid of the box moving gradually closer to the box body as the magnesium concentration is increased and causing a smaller average distance between the two fluorophores. Sample aggregation is another effect that can occur in solutions containing high salt concentrations as reported by gel analysis for different DNA origami structures.[10, 38] Aggregation can also affect the FRET efficiency by bringing donor and acceptor on different DNA boxes closer together, or by distorting or maybe even collapsing the structures. To avoid aggregation, DNA boxes were immobilized on a quartz cover glass prior to exposure to high Mg^{2+} concentrations and their local conformation was investigated by smFRET microscopy. In this approach, molecules are detected as fluorescent spots, the intensity of which did not change significantly for different Mg^{2+} concentrations. Thus, using this experimental configuration, it was possible to expose the DNA box to very high Mg^{2+} concentrations and still avoid aggregation. smFRET time traces were collected at different Mg^{2+} concentrations and plotted as single molecule FRET histograms (Figure 3 and Figure S4, ESI). These data showed that the peak value of the FRET signal, which is attributed to arise from closed DNA boxes, increased from ~0.15 to ~0.4 with increasing Mg^{2+} concentration. This observation is consistent with Mg^{2+} shielding the negative charges in the DNA backbone, and thus having the lid of the box move closer to the box body. The presence of magnesium has previously been shown to compact DNA origami plates with the strongest effect observed perpendicularly to the DNA helices direction of the origami and no compaction observed in the parallel direction.[39] In the DNA box, DNA helices are not oriented in the same direction on each face (Figure 2b and Figure 3a), and thus magnesium could possibly also affect the global box structure. At very high Mg^{2+} concentrations (150 mM and above) (Figure 3b and Figure S4, ESI), a weak separate peak appeared centered around a FRET efficiency of zero. This peak arises from boxes where donor and acceptor fluorophores are more than 10 nm away from each other and can represent open, collapsed or heavily distorted boxes. A significant population of closed DNA boxes with a FRET efficiency peak at ~ 0.4 was observed even at 1 M Mg^{2+} where, upon addition of keys for opening of the box, the FRET efficiency decreased to nearly zero (Figure 3b). Thus the box is still functional even at the highest Mg^{2+} concentration. After exposing the DNA boxes to high magnesium concentration (≤250 mM Mg^{2+}), we exchanged the buffer to return to our start value of 12.5 mM Mg^{2+}. We observed that the FRET efficiency did not decrease down to its original value of ~0.15 (Figure 3b). This observation could imply that a high magnesium concentration enables the structure and/or local structure of the DNA box to achieve conformations that are stable even when subsequently decreasing the salt concentration. Both magnesium concentration and DNA origami shape have been found to affect the DNA origami structural stability.[40, 41]

The flexibility of the single layer of double stranded DNA can contribute to the observed low FRET efficiency for the closed DNA box by causing bulging of the lid or bending of the helix ends on the front face of the DNA origami box. In fact, the donor fluorophore is situated on a helix on the front face of the box that appears from simulations to be spatially fluctuating (Figure 1a and Figure 3a and ESI Movie 1). To investigate this further, the acceptor fluorophore was positioned on a neighboring helix end (Figure 3c). Fluorophores are placed at the end of these helices at a position where, from the box design, there could be a cross-over between these two helices and thus, the two fluorophores should be in very close proximity to each other in the absence of electrostatic repulsion. However, the FRET efficiency of this box was only ~0.3 at 12.5 mM Mg^{2+} (Figure 3d), thus the two ends of the helices are located away from each other, on average. The observed low FRET efficiency is consistent with BD simulation results (Figure S5, ESI) showing fluctuating distances between the two helices with a mean

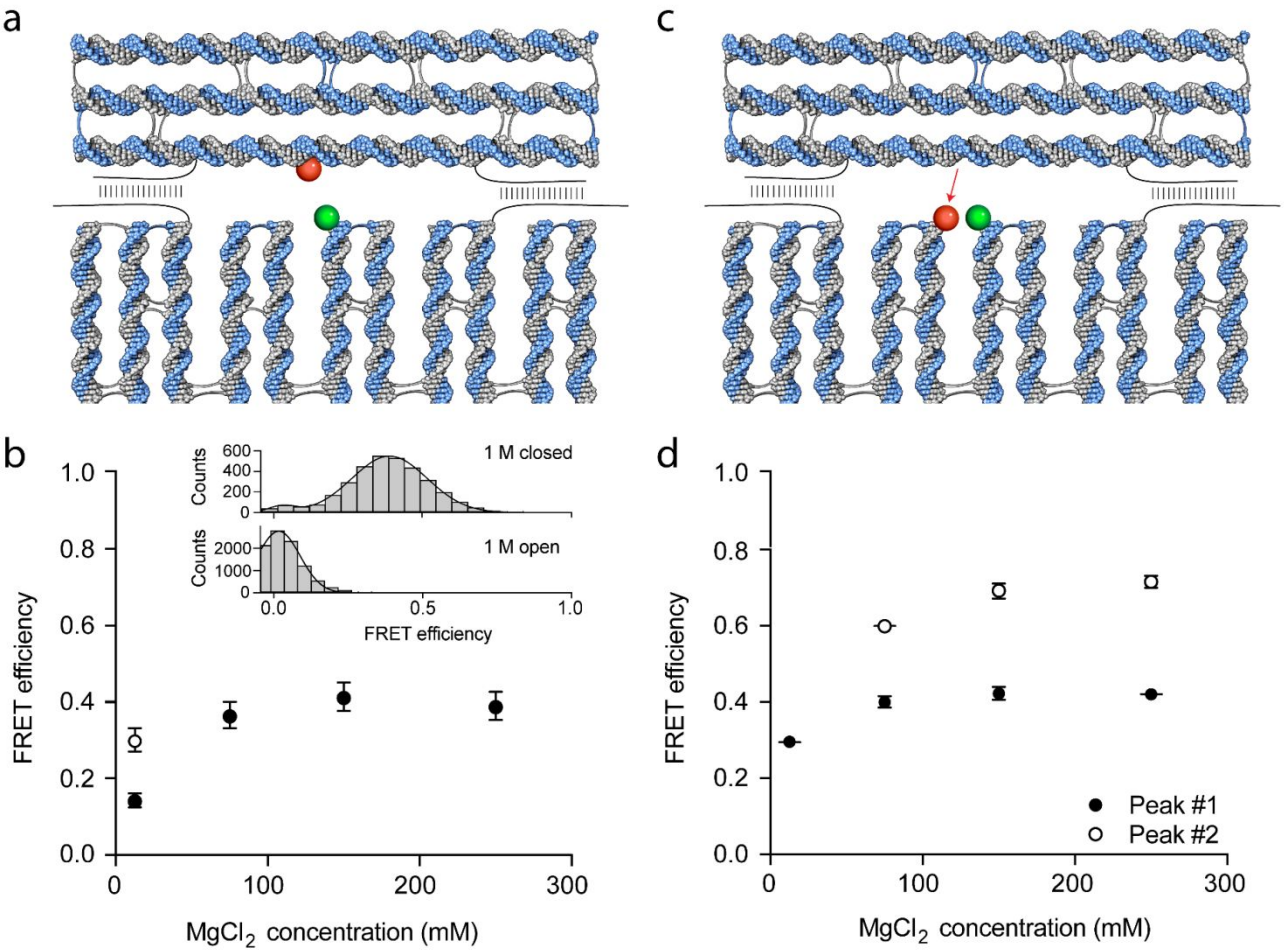

Figure 3: (a) and (c) Schematic view of the lid and front face of the original DNA origami box showing idealized DNA structure (not including DNA bending) and cross-overs and lock positions. The distance between helices was set to 1.2 nm for the upper face and to 0.5 and 1.8 nm for the lower face depending if the helices are linked by a cross-over or not, respectively. The viral DNA scaffold is marked in blue and staple strands are in grey. Donor and acceptor fluorophores, shown in green and red respectively, are placed (a) on different faces (c) on the same face (the red arrow indicates a change in the acceptor position) (b) Peak FRET efficiency of the closed box as a function of increasing Mg^{2+} concentration (filled symbols) for samples with fluorophores on two different faces. The open symbol shows the FRET efficiency at 12.5 mM Mg^{2+} after the samples were exposed to 250 mM Mg^{2+}. Insert: smFRET histograms of the original DNA box in the presence of 1 M Mg^{2+} before and after addition of DNA keys based on 30 and 60 molecules, respectively. (d) Peak FRET efficiencies as a function of increasing Mg^{2+} concentration for samples with fluorophores on the same face.

distance of ~5 nm. The FRET efficiency increased with increasing Mg^{2+} concentration (Figures 3d and Figure S6, ESI) which is attributed to the magnesium decreasing electrostatic repulsions, causing the two ends of the helices to move closer to each other. We furthermore observed the appearance of a small population at higher FRET efficiencies (~ 0.75) at high magnesium concentrations. No dynamic conformational changes between the two FRET states were observed on the time scale of our smFRET experiments. The small high-FRET population, which does not appear in the BD simulations, could arise from a small part of the boxes having a slightly different conformation around the lid. In conclusion, the flexibility of short double-stranded helices on the adjacent face to the lid of the DNA box influences the measured FRET efficiency and affects the local structure around the lid. These fluctuating parts should thus be avoided in applications that use DNA origami for accurate spatial positioning of fluorophores or other ligands, especially at magnesium concentrations below 20-25 mM.

Dependence of FRET efficiency on DNA box design

DNA origami structures can be manipulated by changing staple strands sequence and positions of cross-overs.[42, 43] Small changes, such as adding or deleting staple strand bases can induce significant structural changes, for example by causing structural twisting and curving.[44] We performed small changes to the box design by linking the ends of the helices on the front face of the box that slightly changed the position of the fluorophore and one of the locks (Figure 4a). This change in design led to an increased FRET efficiency of ~0.4, in regular 12.5 mM Mg^{2+} folding buffer, which did not increase significantly with increasing magnesium concentration (Figure 4b and Figure S7, ESI). Linking the ends of the helices together necessitated a minor change to the attachment of the donor

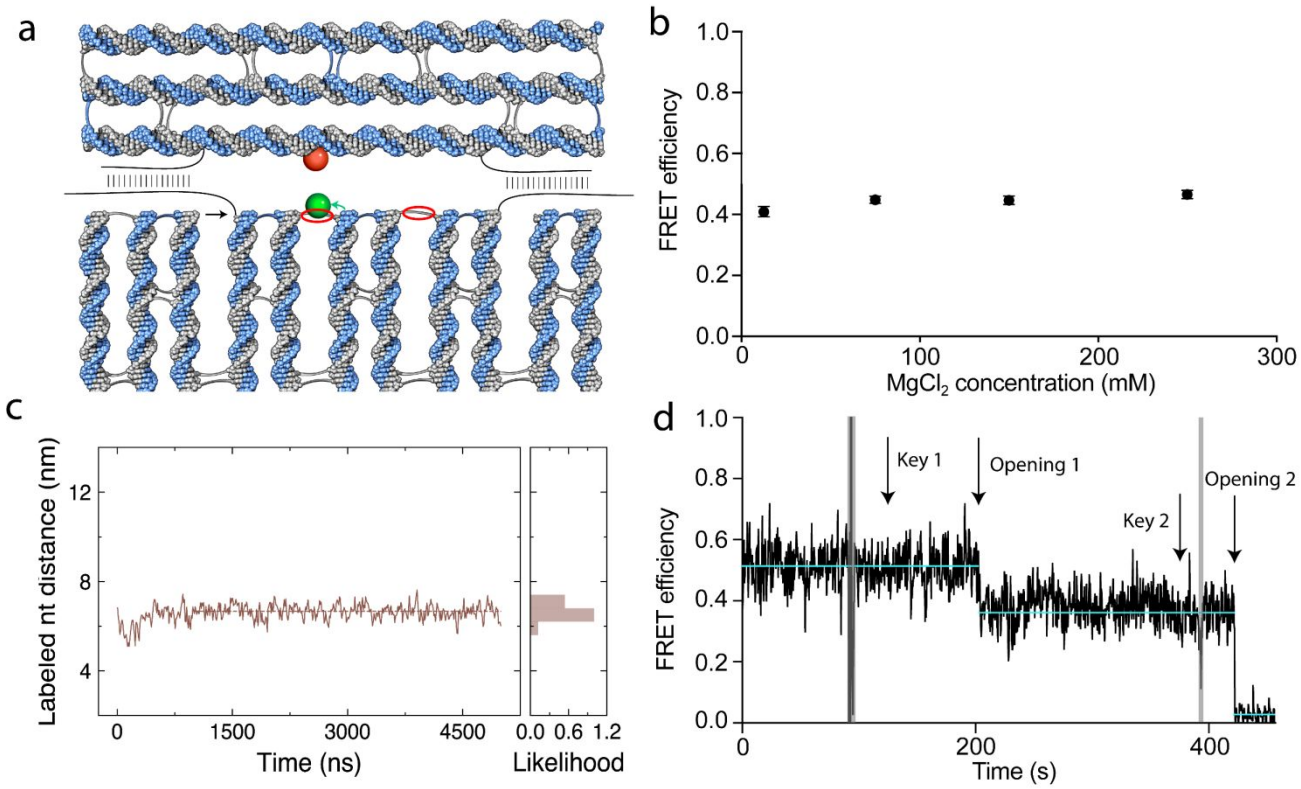

Figure 4: (a) Schematic view of the front face of the end-linked DNA box and of the lid above obtained as described in Figure 3a. The arrows indicate how the lock (black) and donor fluorophore (green) have moved compared to the original box, and the red circles indicate added links in the structure. (b) Peak FRET efficiencies as a function of increasing Mg^{2+} concentration. (c) Time series of the distance between fluorescently labeled nucleotides during a BD simulation of the modified closed box design. The simulation was performed using the same protocol as described for the original box design. The dashed line shows the average value of the distance within the last 4 µs of the 5-µs-long trajectory. The histogram at the right depicts the distribution of the distance during this same time interval. (d) FRET time trace during sequential addition of oligonucleotide keys (indicated by "Key 1" and "Key 2") to an end-linked DNA origami box sample in 12.5 mM $MgCl_2$. The opening steps are indicated by "Opening 1" and "Opening 2". The gray areas indicate acceptor blinking.

fluorophore onto the DNA. In the original design, the donor fluorophore is attached on the 3'-end of a staple strand. But, in the linked box there are no staple strand ends at the edge of the face, and the fluorophore is instead attached internally on a staple strand on an unpaired dT linking two helices. BD simulations show that this small difference in donor attachment position have little effect on the donor/acceptor distance (Figure 4c and Figure S8, Supporting information). The Cy3 donor could still interact differently with the DNA for the different attachment strategies. Terminally-attached fluorophores are indeed likely to stack onto the last DNA base pair of the double stranded DNA, an effect known to influence the FRET efficiency.[31, 45] We used double-stranded control DNA oligonucleotides with Cy3 either attached on the 3'-end or internally to a thymidine to test how the dye position influenced our data (Figure S9, ESI). The FRET efficiency obtained for the two designs was almost the same and did not significantly depend on magnesium concentration. Thus, FRET efficiencies can be compared between the different box designs. We find that, at high magnesium concentrations, values for the helix-linked box (FRET efficiency ~ 0.45) are slightly higher than the FRET efficiency obtained with the original DNA box design (FRET efficiency ~ 0.4).

Cy5 fluorescence quenching, which was seen in the original box design (Figure S2, ESI) was not observed in the case of the linked box design. This observation suggests that quenching is related to interactions between the two fluorophores. Although the average distance between the two fluorophores is large in the original box (Figure 1 and 2), structural flexibility would enable the distance to fluctuate significantly over time allowing fluorophores to briefly come very close together and interact. The BD simulations support this view; in the original design, the fluctuations caused the closest approach of the sites to be below 5 nm (Figure 2e). Although the simulated average distance between the fluorophore attachment sites is slightly larger (~6.5 nm) for the linked box, distance fluctuations are now small (Figure 4c and ESI movie 2). Hence, we see the closest approach of the fluorophore attachment sites in the original box design, which may have caused the observed fluorescence quenching due to fluorophores transiently being very close to each other. Thus, small changes in DNA origami design can reduce structural fluctuations. The linked DNA box provides a much better frame than the original box for accurate positioning of fluorophores and other ligands. Distance fluctuations from BD simulations were indeed below 2 nm and can potentially be further decreased as the face opposite the lid

is not fully linked past DNA locks. Our results imply the potential for a similar position accuracy as more rigid and not dynamically reconfigurable DNA structures.[8] The linked DNA box was fully functional and sequential addition of the two different key oligonucleotides led to a two-step opening of the lid, as reflected in an intermediate FRET state between the fully-open and fully-closed states (Figure 4d). FRET efficiency of the closed box can potentially be increased by further optimising the lock positions, which may also affect the local structure (Supplementary movie 2) and yield an even better closed box. Different designs can be used to create reconfigurable structures. These are often intrinsically less rigid than static structures, which may be caused by fluctuations in their local structure.

Conclusions

Controlling the spatial and temporal arrangement of individual components in macromolecular biological assemblies is an important goal in nanotechnology and synthetic biology.[46] DNA origami structures are interesting tools in the endeavour as they are highly addressable, allow nanoscale organization of matter and can also be designed to be dynamically reconfigurable to enable temporal control and triggering of reactions. Here we report, using single molecule FRET microscopy and BD simulations, that the DNA origami box undergoes local distortions that strongly affect the precision of fluorophore placement. Higher levels of structural control and rigidity are achieved by increasing magnesium concentration and through small modifications to the DNA box design. Our study, combined with recent work showing that the addressability of two dimensional origami structures varied significantly depending on site position,[47] allow for improved rational engineering of DNA nanostructures to achieve more accurate and precise organization of matter in three dimensions.

Conflicts of interest

There are no conflicts to declare.

Acknowledgements

This work was supported by the Danish Council for Independent Research through a Sapere Aude II grant to VB (DFF-0602-01670) and by the Danish National Research Foundation to Center of DNA nanotechnology (DNRF 81) and Center for Cellular Signal Patterns (CellPat). A.A. and C.M. acknowledge support from the National Science Foundation (USA) under Grants DMR- 1827346 and OAC-1740212 and from the US National Institutes of Health under grant P41-GM104601.

Notes and references

1. M. R. Jones, N. C. Seeman and C. A. Mirkin, *Science*, 2015, **347**, 12.
2. F. Zhang, J. Nangreave, Y. Liu and H. Yan, *J. Am. Chem. Soc.*, 2014, **136**, 11198-11211.
3. L. L. Hildebrandt, S. Preus, Z. Zhang, N. V. Voigt, K. V. Gothelf and V. Birkedal, *J. Am. Chem. Soc.*, 2014, **136**, 8957-8962.
4. E. S. Andersen, M. Dong, M. M. Nielsen, K. Jahn, R. Subramani, W. Mamdouh, M. M. Golas, B. Sander, H. Stark, C. L. P. Oliveira, J. S. Pedersen, V. Birkedal, F. Besenbacher, K. V. Gothelf and J. Kjems, *Nature*, 2009, **459**, 73-75.
5. S. M. Douglas, I. Bachelet and G. M. Church, *Science*, 2012, **335**, 831-834.
6. Y. Amir, E. Ben-Ishay, D. Levner, S. Ittah, A. Abu-Horowitz and I. Bachelet, *Nat. Nanotechnol.*, 2014, **9**, 353-357.
7. R. M. Zadegan, M. D. E. Jepsen, L. L. Hildebrandt, V. Birkedal and J. Kjems, *Small*, 2015, **11**, 1811-1817.
8. J. J. Funke and H. Dietz, *Nat. Nanotechnol.*, 2016, **11**, 47-52.
9. Y. G. Ke, J. Sharma, M. H. Liu, K. Jahn, Y. Liu and H. Yan, *Nano Lett.*, 2009, **9**, 2445-2447.
10. R. M. Zadegan, M. D. E. Jepsen, K. E. Thomsen, A. H. Okholm, D. H. Schaffert, E. S. Andersen, V. Birkedal and J. Kjems, *Acs Nano*, 2012, **6**, 10050-10053.
11. A. Kuzuya and M. Komiyama, *Chemical Communications*, 2009, 4182-4184.
12. G. Grossi, M. D. E. Jepsen, J. Kjems and E. S. Andersen, *Nat. Commun.*, 2017, **8**, 8.
13. G. Grossi, A. Jaekel, E. S. Andersen and B. Sacca, *MRS Bull.*, 2017, **42**, 920-924.
14. F. Hong, F. Zhang, Y. Liu and H. Yan, *Chem. Rev.*, 2017, **117**, 12584-12640.
15. V. Birkedal, M. Dong, M. M. Golas, B. Sander, E. S. Andersen, K. V. Gothelf, F. Besenbacher and J. Kjems, *Microscopy Research and Technique*, 2011, **74**, 688-698.
16. B. Sacca, Y. Ishitsuka, R. Meyer, A. Sprengel, E. C. Schoneweiss, G. U. Nienhaus and C. M. Niemeyer, *Angewandte Chemie-International Edition*, 2015, **54**, 3592-3597.
17. P. C. Nickels, B. Wunsch, P. Holzmeister, W. Bae, L. M. Kneer, D. Grohmann, P. Tinnefeld and T. Liedl, *Science*, 2016, **354**, 305-307.
18. R. S. Sorensen, A. H. Okholm, D. Schaffert, A. L. B. Kodal, K. V. Gothelf and J. Kjems, *Acs Nano*, 2013, **7**, 8098-8104.
19. R. M. Clegg, *Methods Enzymol.*, 1992, **211**, 353-388.
20. S. Preus, S. L. Noer, L. L. Hildebrandt, D. Gudnason and V. Birkedal, *Nat Methods*, 2015, **12**, 593-594.
21. L. L. Hildebrandt, S. Preus and V. Birkedal, *Faraday Discuss.*, 2015, **184**, 131-142.
22. J. Comer and A. Aksimentiev, *The Journal of Physical Chemistry C*, 2012, **116**, 3376-3393.
23. E. A. Hemmig, C. Fitzgerald, C. Maffeo, L. Hecker, S. E. Ochmann, A. Aksimentiev, P. Tinnefeld and U. F. Keyser, *Nano Lett.*, 2018, **18**, 1962-1971.
24. S. M. Douglas, A. H. Marblestone, S. Teerapittayanon, A. Vazquez, G. M. Church and W. M. Shih, *Nucleic Acids Research*, 2009, **37**, 5001-5006.
25. F. Mosconi, J. F. Allemand, D. Bensimon and V. Croquette, *Phys. Rev. Lett.*, 2009, **102**, 078301.
26. D. J. Kauert, T. Kurth, T. Liedl and R. Seidel, *Nano Lett.*, 2011, **11**, 5558-5563.
27. J. Yoo and A. Aksimentiev, *Nucleic Acids Res.*, 2016, **44**, 2036-2046.
28. S. M. Slone, C. Y. Li, J. Yoo and A. Aksimentiev, *New J Phys*, 2016, **18**.
29. R. Zwanzig, *P Natl Acad Sci USA*, 1988, **85**, 2029-2030.
30. N. Di Fiori and A. Meller, *Biophys. J.*, 2010, **98**, 2265-2272.

31. A. Iqbal, S. Arslan, B. Okumus, T. J. Wilson, G. Giraud, D. G. Norman, T. Ha and D. M. J. Lilley, *Proc. Natl. Acad. Sci. U. S. A.*, 2008, **105**, 11176-11181.
32. E. Lerner, E. Ploetz, J. Hohlbein, T. Cordes and S. Weiss, *Journal of Physical Chemistry B*, 2016, **120**, 6401-6410.
33. Y. Gidi, M. Gotte and G. Cosa, *Journal of Physical Chemistry B*, 2017, **121**, 2039-2048.
34. T. Schroder, M. B. Scheible, F. Steiner, J. Vogelsang and P. Tinnefeld, *Nano Lett.*, 2019, **19**, 1275-1281.
35. C. Agbavwe and M. M. Somoza, *PLoS One*, 2011, **6**, 10.
36. T. Cordes, Y. Santoso, A. I. Tomescu, K. Gryte, L. C. Hwang, B. Camara, S. Wigneshweraraj and A. N. Kapanidis, *Biochemistry*, 2010, **49**, 9171-9180.
37. D. Cauchy, R. Lavery and B. Pullman, *Theor. Chim. Acta*, 1980, **57**, 323-327.
38. W. M. Shih, S. M. Douglas, H. Dietz, T. Liedl, B. Hogberg and F. Graf, *Journal of Biomolecular Structure & Dynamics*, 2009, **26**, 799-799.
39. C. Y. Li, E. A. Hemmig, J. L. Kong, J. Yoo, S. Hernandez-Ainsa, U. F. Keyser and A. Aksimentiev, *Acs Nano*, 2015, **9**, 1420-1433.
40. C. Kielar, Xin, Y.; Shen, B.; Kostiainen, M.A.; Grundmeier, G.; Linko, V.; Keller, A., *Angew Chem Int Ed Engl.*, 2018, **57**, 9470-9474.
41. S. Fischer, C. Hartl, K. Frank, J. O. Radler, T. Liedl and B. Nickel, *Nano Lett.*, 2016, **16**, 4282-4287.
42. P. W. K. Rothemund, *Nature*, 2006, **440**, 297-302.
43. R. Kosinski, A. Mukhortava, W. Pfeifer, A. Candelli, P. Rauch and B. Sacca, *Nat. Commun.*, 2019, **10**, 12.
44. H. Dietz, S. M. Douglas and W. M. Shih, *Science*, 2009, **325**, 725-730.
45. S. Sindbert, S. Kalinin, N. Hien, A. Kienzler, L. Clima, W. Bannwarth, B. Appel, S. Muller and C. A. M. Seidel, *J. Am. Chem. Soc.*, 2011, **133**, 2463-2480.
46. B. A. Grzybowski and W. T. S. Huck, *Nat. Nanotechnol.*, 2016, **11**, 584-591.
47. M. T. Strauss, F. Schueder, D. Haas, P. C. Nickels and R. Jungmann, *Nat. Commun.*, 2018, **9**, 7.

Single Molecule Analysis of Structural Fluctuations in DNA Nanostructures

Mette D. E. Jepsen[1,2], Rasmus Schøler Sørensen[1,2], Christopher Maffeo[3], Aleksei Aksimentiev[3], Jørgen Kjems[1,2], Victoria Birkedal[1,4*]

Table of Contents

The local structure of DNA origami boxes shows fluctuations, visualized through single molecule FRET and coarse grain Brownian dynamics.

ToC figure